

## Analytical prediction of chatter stability for modulated turning

Soohyun Nam <sup>a,\*</sup>, Bora Eren <sup>b</sup>, Takehiro Hayasaka <sup>a</sup>, Burak Sencer <sup>b</sup>, Eiji Shamoto <sup>a</sup>

<sup>a</sup> Department of Aerospace Engineering, Graduate School of Engineering, Nagoya University, Furo-cho, Chikusa-ku, Nagoya, 464-8603, Japan

<sup>b</sup> School of Mechanical, Industrial and Manufacturing Engineering, College of Engineering, Oregon State University, Corvallis, OR, USA



### ARTICLE INFO

#### Keywords:

Turning  
Chatter  
Low frequency vibration  
Stability lobe diagram  
Multi-delay regeneration

### ABSTRACT

This paper proposes an analytical chatter stability prediction for low frequency vibration assisted turning process, i.e. the modulated turning. Introducing low frequency tool modulations in machining is initially proposed to transform continuous cutting process into a discrete one so that chip-entanglement/jam could be eliminated. However, tool modulation assistance has a fundamental effect on chatter stability. This paper is the first attempt to uncover the regenerative chatter stability of the modulated turning process by a frequency-domain analysis. Tool engagement kinematics and the dynamic chip generation mechanism are modeled. It is understood that unlike conventional turning or milling processes, modulated turning process exhibits distinct stabilizing effects due to 1) short-time tool engagement and 2) multiple regenerative loops as the dynamic chip thickness is affected by past two revolutions. Considering the average immersion of the cutting tool (cutting duty cycle), a zero-th order frequency domain chatter stability model for the process is proposed. The developed model is used to quantify the effect of multi-delay regeneration and tool modulation parameters on the stability loop formation. The analytical stability solutions are benchmarked against the time domain digital simulation results, and both predictions are validated through orthogonal cutting experiments. It is shown that the proposed solution can accurately generate the Stability Lobe Diagram (SLD) of modulated turning for typical modulation conditions.

### 1. Introduction

Continuous cutting processes such as turning, boring, drilling or threading operations suffer from a well-known disruption the so-called “chip-jam” or “chip-entanglement” [1,2]. Chip-jam occurs especially while machining ductile materials since long continuous chips cannot be broken easily. They tangle around the cutting zone and easily jam around the cutting zone. Chip-jam not only disrupts process automation, but also causes tool breakage, poor surface finish, and workplace injuries [2]. The most well-known approach to eliminate chip-jam is to utilize tools with chip breaker geometries [1–4]. Chip breakers are generally effective only around an optimal operating (design) point. Also note that due to lack of accurate simulation models, a lengthy trial-and-error based tuning process may be needed to identify this optimal chip-breaker operating point [4]. Therefore, application of high-pressure coolant [5] and other innovative chip deposition systems have been proposed in the literature [6,7].

A fundamental cure to the chip jam is to convert the continuous cutting process into discontinuous cutting so that discrete chip can be generated. Modulation assisted cutting process has been originally

proposed to serve this purpose. It is firstly proposed for deep hole drilling [8] in an attempt to assist chip evacuation. Later, it has been adopted to turning [9,10] and threading [11] processes to eliminate the chip jam. Fig. 1 illustrates kinematics of modulated turning. As shown, the tool is modulated (vibrated) sinusoidally in feed direction at low frequency. When modulation frequency to the spindle rotation frequency ratio is not integer and modulation amplitude is larger than nominal feed rate, the tool starts to disengage from the workpiece in successive spindle revolutions. As a result, continuous turning kinematics is altered to “discontinuous turning”, which inherently generates discrete chip and thus eliminates the chip jam problem.

Past literature focused on the kinematics of this modulated turning process [12–17]. Modulation frequency and amplitude play a key role in realizing discrete turning. Discrete chip generation lobes are generated, which indicate under what modulation conditions discrete chip could be generated [15,16]. It is understood that the most efficient modulation condition is when the modulation frequency is selected half of the spindle rotation frequency and when the modulation amplitude is half of the nominal feed rate in turning. Such low frequency modulation allows modulated turning to be applied by the machine's own servo drives and

\* Corresponding author.

E-mail address: [nam@upr.mech.nagoya-u.ac.jp](mailto:nam@upr.mech.nagoya-u.ac.jp) (S. Nam).

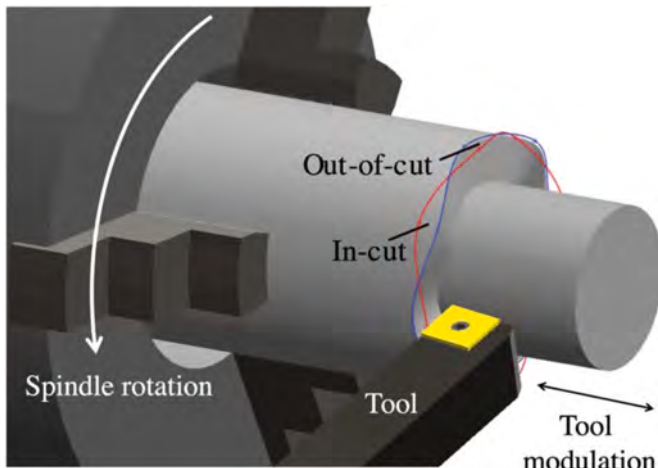


Fig. 1. Schematic illustration of modulated turning.

axes [18]. Therefore, in practice, modulated turning can be applied without any external devices or actuators. Discrete chip generation maps for modulated turning or drilling process are also available. Note that modulated drilling process is also known as the “drilling with pecking cycles” and well adopted in machining industries [12,19–21].

Apart from its kinematics, the mechanics of modulated turning process has also been investigated [15,17,22]. Gao et al. [23] has developed models to predict cutting forces in modulated turning. The simplest model has been proposed by Copenhagen et al. [9,10], and later Eren et al. [24] who have adopted very simple mechanistic cutting force models with constant cutting force coefficients to predict machining forces in modulated turning. The uncut chip thickness is computed from kinematics of the process. It has been revealed that even at low nominal feed and modulation conditions, simple mechanistic cutting force models can accurately predict cutting forces in modulated turning. Others have developed more sophisticated models that capture shear deformation in the primary and secondary cutting zones and also the thermal effects [23,25]. It is shown that modulated turning can reduce specific cutting energy and improve machineability [14,24,26]. On a different note, past literature has also shown that modulated turning can provide lower machining temperatures [9,27] and better tool life [14]. Owing to its ability to disengage the tool from cutting zone it allows the tool to cool down, which helps with the thermal wear and elongates overall tool life [14].

Dynamic stability of the cutting process is critical for achieving greater material removal rates in modulated turning. The stability in turning processes is mainly governed by regenerative chatter vibrations that are triggered due to flexibilities in the workpiece or the tool [28–32]. In particular, due to continuous cutting kinematics in conventional turning, chatter vibrations quickly onset and rapidly grow once the tool or the workpiece is perturbed/vibrated. Accurate stability prediction methods [29] and solution for mitigation of chatter vibrations [31,32] in continuous turning process have been extensively studied. However, by the addition of tool modulations, continuous turning becomes interrupted in modulated turning, and it resembles dynamics of a milling process [29,33]. Copenhagen et al. [34] was the first one to report the stability gain in modulated turning as compared to continuous cutting. They developed a time-domain model to simulate modulated turning process and validated the chatter stability experimentally [10]. However, time-domain models can only be used to test stability of the process in a point-by-point basis. This is mostly due to the time-consuming nature of running time domain simulations. More importantly, time-domain simulations do not provide critical engineering insight on how process parameters affect chatter stability and the overall dynamics of the process. Therefore, analytical prediction of stability lobes is necessary to generate stability lobe diagrams (SLD) for

the modulated turning process and plan for better productivity.

In this paper, an analytical approach for chatter stability prediction in modulated turning is proposed for the first time, and the reasons for the stabilizing effect by tool modulations are uncovered. Firstly, kinematics of modulated turning is considered, and frequency domain based analytical prediction of regenerative chatter stability model is presented. These frequency domain stability predictions are validated against the time domain simulations. This is then followed by analytical investigations into the effects of modulation parameters on the chatter stability and the magnitude of stabilizing factors. Experimental results in the form of orthogonal (plunge) turning tests are provided to validate the developed model.

## 2. Analytical chatter stability of modulated turning

### 2.1. Process kinematics and prediction of uncut chip thickness

This section first introduces basic kinematics of modulated turning and the prediction of uncut chip thickness. Discrete chip generation in modulated turning is controlled by the tool modulation frequency and amplitude [16]. Fig. 2(a) shows a 2-D model of the process. Tool is

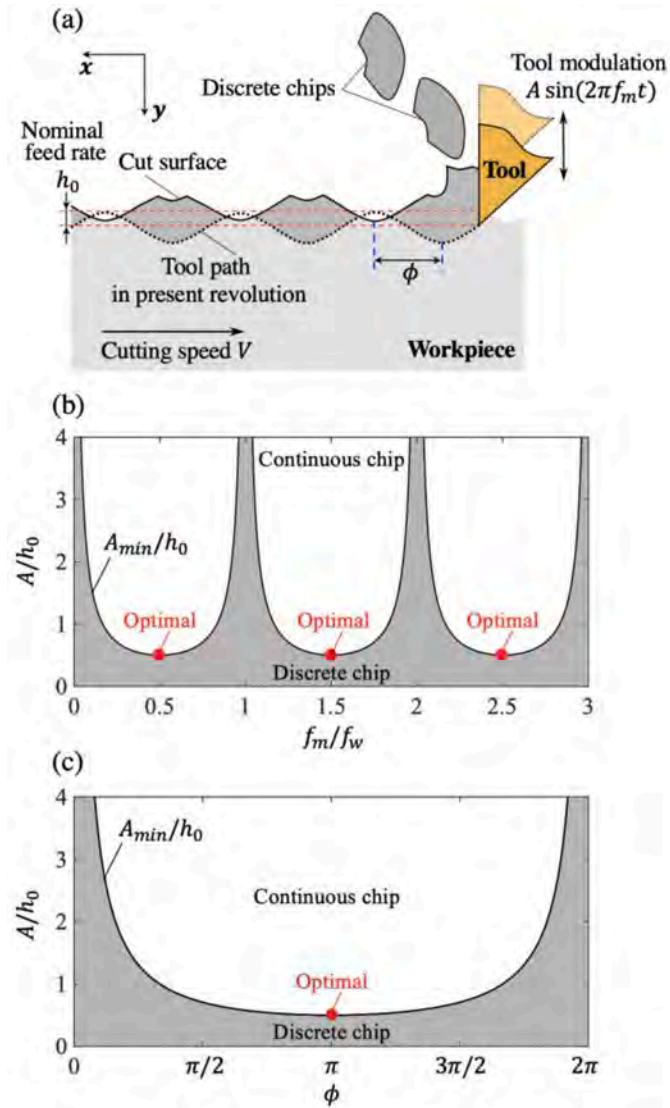


Fig. 2. (a) 2-D model of modulated turning, (b) Discrete chip generation map against modulation parameters, and (c) Discrete chip generation map against phase difference between two consecutive tool trajectories.

modulated (vibrated) sinusoidally in the feed direction by:

$$M(t) = A \sin(2\pi f_m t) \quad (1)$$

where  $A$  [m] is the modulation amplitude and  $f_m$  [Hz] is the modulation frequency. Combined with the tool's normal (static) feed rate  $h_0$  [m], the total tool trajectory in feed direction can be expressed as:

$$Y(t) = h_0 f_w t + A \sin(2\pi f_m t) \quad (2)$$

where  $f_w$  [Hz] is the spindle rotation frequency. Note that  $f_w = n / 60$  where  $n$  [min<sup>-1</sup>] is the spindle speed. The uncut chip thickness varies due to the tool modulation, and it can be expressed as the difference of tool trajectories between present and past revolutions as:

$$h_m(t) = Y(t) - \max\{Y(t - \tau), Y(t - 2\tau), \dots\} \quad (3)$$

where  $\tau = 1/f_w$  is the spindle rotational period. As shown in the shaded region in Fig. 2(a), for certain modulation amplitude-nominal feed rate ratio  $A/h_0$  and modulation frequency-spindle frequency ratio  $f_m/f_w$ , the uncut chip thickness can become zero or even negative. Negative chip thickness indicates that continuous turning process is transformed into discrete cutting. The smallest modulation amplitude that ensures discrete cutting can be computed by searching for the intersection of current and past tool trajectories. For instance, considering the current and the previous tool trajectories and setting  $Y(t) = Y(t - \tau)$  yields the minimum modulation amplitude  $A_{min}$  that ensures discrete chip generation as:

$$A_{min} = \frac{h_0}{2 \sin\left(\frac{\varphi}{2}\right)} \quad (4)$$

Where  $\varphi$  [rad] is the phase angle between consecutive tool modulation trajectories and defined as [12,14–16,24]:

$$\varphi = 2\pi \left( \frac{f_m}{f_w} - \text{int}\left[ \frac{f_m}{f_w} \right] \right), \quad (0 \leq \varphi < 2\pi) \quad (5)$$

where  $\text{int}[\cdot]$  function takes the integer part of the rational value. Notice that a critical condition for discrete chip generation is that the phase angle must be  $\varphi \in (0, 2\pi)$ . Otherwise, consecutive modulation waves are in phase and a continuous (conventional) turning process is realized that leaves a wavy surface finish. Fig. 2(b) and (c) depict the minimum modulation amplitude-nominal feed ratio  $A_{min}/h_0$  ratio w.r.t to  $f_m/f_w$  and  $\varphi$  based on Eq. (5). As shown, any modulation amplitude smaller than the border line ensures that discrete chip generation is observed. These maps are referred as the discrete chip generation maps [16]. Considering optimal points in Fig. 2(b) and (c),  $A_{min}$  has the smallest value under  $\varphi = \pi$  ( $f_m/f_w = 0.5, 1.5, 2.5, \dots$ ). This denotes that discrete chips can be obtained with the smallest modulation amplitude under  $\varphi = \pi$ , and least amount of energy is required to realize it. Therefore, modulation conditions satisfying this particular phase angle are most favorable and employed in practice as well [10]. This section focuses on modeling the modulated turning process for this optimal phase angle condition ( $\varphi = \pi$ ).

Assuming that discrete cutting is realized at this optimal operating condition, uncut chip thickness can be predicted analytically as follows. Fig. 3 shows the tool trajectory and the uncut chip thickness during 4 consecutive spindle revolutions for the phase angle  $\varphi = \pi$ . The shaded areas indicate the uncut chip thickness portion. As shown, current tool trajectory in  $(N)^{th}$  spindle revolution intersects with the previous tool trajectory in  $(N-1)^{th}$  spindle revolution. Similarly, the  $(N-1)^{th}$  tool trajectory intersects with the  $(N-2)^{th}$  and so on. As depicted in the figure, this results in an uncut chip thickness, which consist of 3 different portions. Firstly, the chip thickness increases between  $\theta_1$  and  $\theta_2$  (Section A) where it is formed by the current tool trajectory in the  $N^{th}$  spindle revolution and the surface that is left in the previous  $(N-1)^{th}$  spindle

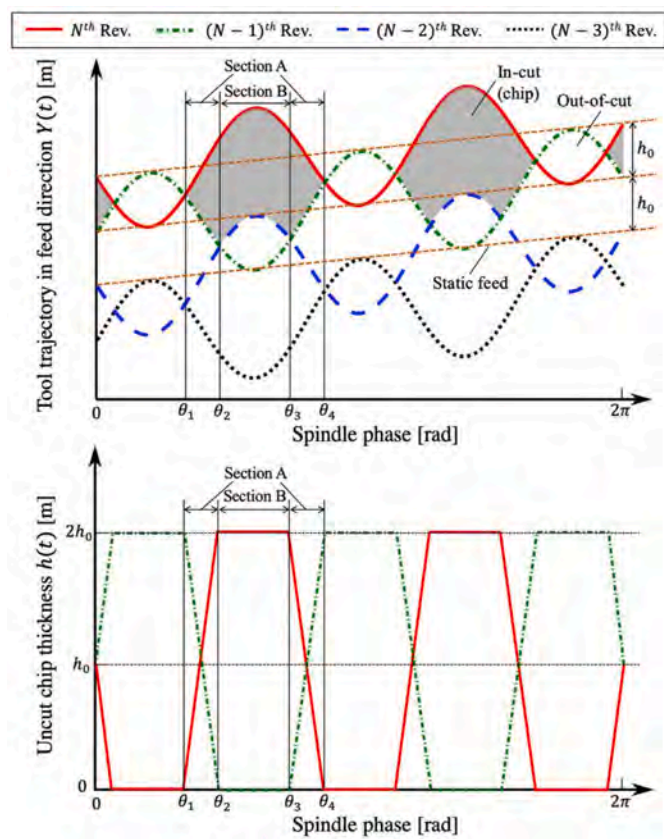


Fig. 3. Tool trajectory and uncut chip thickness against spindle phase during modulated turning under  $\varphi = \pi$ .

revolution. Next, between  $\theta_2$  and  $\theta_3$  (Section B), chip thickness is constant, and it doubles the nominal feed rate,  $2h_0$ . Notice that in this region, chip is being formed by the current tool trajectory and the surface generated 2 spindle revolutions before, i.e., during  $(N-2)^{th}$  spindle revolution. Finally, the chip thickness decreases between  $\theta_3$  and  $\theta_4$  and the chip is again generated between two consecutive spindle revolutions. The spindle angular positions  $\theta_1, \theta_2, \theta_3$ , and  $\theta_4$  can be computed by searching for the intersection of tool trajectories in  $(N)^{th}$ ,  $(N-1)^{th}$ , and  $(N-2)^{th}$  spindle revolutions from Eq. (2) as:

$$\begin{cases} \theta_1 = \frac{f_w}{f_m} \left( \pi - \sin^{-1} \frac{h_0}{2A} \right) \\ \theta_2 = \frac{f_w}{f_m} \left( \pi + \sin^{-1} \frac{h_0}{2A} \right) \\ \theta_3 = \frac{f_w}{f_m} \left( 2\pi - \sin^{-1} \frac{h_0}{2A} \right) \\ \theta_4 = \frac{f_w}{f_m} \left( 2\pi + \sin^{-1} \frac{h_0}{2A} \right) \end{cases} \quad (6)$$

where  $|\theta_2 - \theta_1| = |\theta_4 - \theta_3|$ . Also note that the tool loses its contact with the workpiece and undergoes an air-cutting duration between the uncut chip thickness sections.

## 2.2. Regenerative dynamics and frequency domain chatter stability prediction

Based on the chip formation kinematics, a frequency-domain chatter stability prediction of modulated turning is developed as follows. Firstly, it is assumed that the tool shank is flexible in the feed ( $y$ ) direction and the phase angle is set to  $\varphi = \pi$ . When the tool is modulated, sinusoidal rigid body motion of the tool is superimposed with the dynamic vibra-

tion induced by the interaction of the cutting forces with the flexible tool structure. These structural vibrations leave a wavy cut surface. When cutting such wavy surface in successive spindle revolutions, the phase shift between current and past vibrations generates a dynamic chip load. The dynamic chip load, in return, excites the flexible tool and triggers regenerative chatter vibrations that exponentially grow at a chatter frequency. Fig. 4 illustrates the dynamic model of orthogonal modulated turning process.

For modulated turning process, the regeneration mechanism is different than the one found in conventional turning. In conventional turning, typically a single regeneration (delay) causes chatter instability [29–32,35]. However, in modulated turning, uncut chip thickness is influenced by multiple past spindle revolutions. To be exact, uncut chip thickness is governed by the current tool trajectory and the surface generated by the tool trajectory during the two previous spindle revolutions. Notice from Fig. 3 that the first and the last portions of the chip (Section A) are generated by the current tool trajectory and the surface generated in the previous spindle revolution. This is called by “single-delay regeneration” in this paper, and the chip thickness generated in this chip segment is represented by  $h_S$  [m]. On the other hand, the middle portion of the chip (Section B) is formed by the current tool trajectory and the workpiece surface left two revolutions before. This is called as “multi-delay regeneration” in this paper, and the chip thickness generated in this chip segment is represented by  $h_M$  [m]. Once a single discrete chip is cut, the tool flies over a portion of the workpiece until the next chip is formed. Therefore, an air cutting portion is also observed.

The uncut chip thickness in Sections A and Section B can be expressed as:

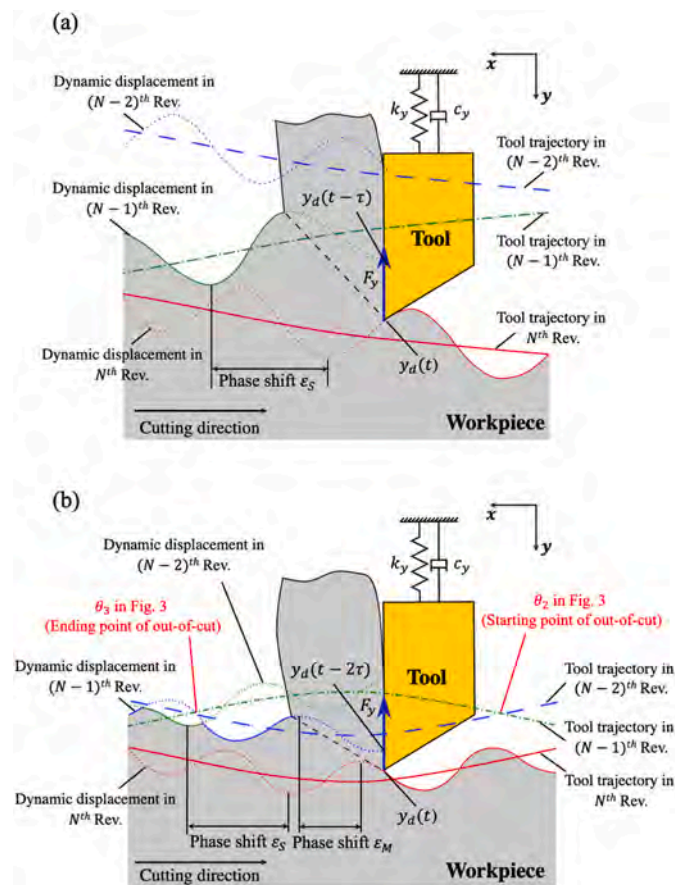


Fig. 4. Dynamic model of orthogonal cutting with modulated turning under  $\varphi = \pi$ : (a) Section A (only single-delay regeneration), (b) Section B (single-delay and multi-delay regenerations).

$$h_S(t) = h_m(t) - h_{d,S}(t) = \{Y(t) - Y(t - \tau)\} - \{y_d(t) - y_d(t - \tau)\} \quad (7)$$

$$h_M(t) = h_m(t) - h_{d,M}(t) = \{Y(t) - Y(t - 2\tau)\} - \{y_d(t) - y_d(t - 2\tau)\}$$

where  $h_{d,S}(t)$  [m] is the dynamic uncut chip thickness due to the cutting process in Section A, and  $h_{d,M}(t)$  [m] is in Section B.  $y_d(t)$  [m] is the dynamic tool displacement. Stability of the system can be evaluated by considering only the dynamic chip thickness with single and multiple delay portions since the quasi-static chip thickness  $h_m(t)$  is due to the rigid body motion of the tool and does not affect chatter growth. The phase shift between previous and present dynamic vibrations in the section where the multi-delay regenerative effect occurs ( $\varepsilon_M$  in Fig. 4(b)) is different from the section where the single-delay regenerative effect occurs ( $\varepsilon_S$  in Fig. 4(a)). These two different phase shifts  $\varepsilon_S$  [rad] and  $\varepsilon_M$  [rad] can be expressed as:

$$\varepsilon_S = \omega_c \tau \quad (8)$$

$$\varepsilon_M = 2\omega_c \tau$$

where  $\omega_c$  [rad/s] is the angular chatter frequency.

Due to the discrete cutting kinematics of modulated turning, tool disengages from workpiece. Such disengagement may have a stabilizing effect on the system since the in-cut section decreases and the regenerative vibrations may be damped during the time while the tool is flying over sections of the workpiece. The angular length of single-delay regenerative section  $\theta_S$ , multiple-delay regenerative section  $\theta_M$ , and out-of-cut sections  $\theta_O$  can be calculated as:

$$\theta_S = 2(\theta_2 - \theta_1) \left( 2 \times \text{int} \left[ \frac{f_m}{f_w} \right] + 1 \right) \quad (9)$$

$$\theta_M = (\theta_3 - \theta_2) \left( 2 \times \text{int} \left[ \frac{f_m}{f_w} \right] + 1 \right)$$

$$\theta_O = 4\pi - \{(\theta_3 - \theta_2) + 2(\theta_2 - \theta_1)\} \left( 2 \times \text{int} \left[ \frac{f_m}{f_w} \right] + 1 \right)$$

Note that  $\theta_S + \theta_M + \theta_O = 4\pi$  since the chip formation cycle repeats itself every 2 spindle revolutions. In other words, a full chip formation cycle (modulation cycle) requires 2 full spindle revolutions since the middle portion of the chip is generated due to the surface left from 2 spindle revolutions before. The ratio of  $\theta_S$ ,  $\theta_M$ , and  $\theta_O$  per one chip formation cycle can be expressed from Eq. (9) as:

$$r_S = \frac{\theta_S}{\theta_S + \theta_M + \theta_O} = \frac{\theta_S}{4\pi} \quad (10)$$

$$r_M = \frac{\theta_M}{\theta_S + \theta_M + \theta_O} = \frac{\theta_M}{4\pi}$$

$$r_O = \frac{\theta_O}{\theta_S + \theta_M + \theta_O} = \frac{\theta_O}{4\pi}$$

Note that  $r_S + r_M + r_O = 1$ . The ratio of the in-cut section per one cycle becomes  $r_S + r_M$ . Since the dynamic cutting force does not occur during the out-of-cut section, dynamic cutting force in that section should not contribute to the regeneration effect. When considering only the in-cut section per one cycle, the normalized ratios  $\bar{r}_S$  and  $\bar{r}_M$ , which express the ratios of  $r_S$  and  $r_M$  to the ratio of the in-cut section per one cycle, are defined as:

$$\bar{r}_S = \frac{r_S}{r_S + r_M} \quad (11)$$

$$\bar{r}_M = \frac{r_M}{r_S + r_M}$$

Equivalent dynamic chip thickness in each modulation cycle  $h_{d,e}$  is expressed by utilizing  $\bar{r}_S$  and  $\bar{r}_M$  from Eqs. 8–11 as:

$$h_{d,e} = \bar{r}_S y_d(e^{-i\varepsilon_S} - 1) + \bar{r}_M y_d(e^{-i\varepsilon_M} - 1) \quad (12)$$

and the equivalent dynamic cutting force in each modulation cycle  $F_{y,e}$  comes:

$$F_{y,e} = (r_s + r_M) K_y b h_{d,e} \quad (13)$$

where  $K_y$  [MPa] is the specific cutting force in the thrust direction, and  $b$  [m] is the cutting width.

Dynamic cutting force excites the structure and generates dynamic tool displacement by:

$$y_d = F_{y,e} \Phi = (r_s + r_M) K_y b h_{d,e} \Phi \quad (14)$$

where  $\Phi$  [m/N] is the frequency response function of the vibratory structure. Overall block diagram of the process is illustrated in Fig. 5. Combining Eqs. (12) and (14), the characteristic equation can be postulated under the critical cutting width  $b_{lim}$  [m] as:

$$y_d(i\omega_c) = (r_s + r_M) K_y b_{lim} y_d(i\omega_c) \{ \bar{r}_s(e^{-i\omega_s} - 1) + \bar{r}_M(e^{-i\omega_M} - 1) \} \Phi(i\omega_c) \quad (15)$$

As a result,  $b_{lim}$  becomes:

$$b_{lim} = \frac{1}{(r_s + r_M) \{ \bar{r}_s(e^{-i\omega_s} - 1) + \bar{r}_M(e^{-i\omega_M} - 1) \} K_y \Phi(i\omega_c)} \quad (16)$$

Note that  $b_{lim}$  is mainly affected by  $(r_s + r_M)$  and  $\{ \bar{r}_s(e^{-i\omega_s} - 1) + \bar{r}_M(e^{-i\omega_M} - 1) \}$  in Eq. (16) since  $K_y$  and  $\Phi(i\omega_c)$  are fixed values that depend mainly on the tool/workpiece and flexibility of the dynamic structure. The magnitude of the stabilizing effect due to those two factors are investigated in the following sections. Note that the size effect of the cutting tool, i.e., the tool edge is generally round and the average rake angle that affects the cutting becomes negative when the uncut chip thickness is small, is not explicitly considered in this paper, but rather included in the specific cutting force coefficients.

### 2.3. Time-domain simulation of regenerative process dynamics

Time-domain simulations are carried out to verify effectiveness of the proposed frequency-domain chatter stability predictions. This section presents the time-domain simulation model, which is used to benchmark the accuracy of frequency domain analysis presented in the previous section.

A single degree of freedom (SDOF) vibratory system in an orthogonal turning process with feed modulations under  $\varphi = \pi$  is assumed. Equation of motion of the cutting tool due to the tool modulation and the cutting process shown in Fig. 4 can be described as:

$$m\ddot{y}(t) + c\dot{y}(t) + ky(t) = K_y b h(t) \quad (17)$$

where  $m$  [kg] is the modal mass,  $c$  [N/(m·s)] is the modal damping coefficient,  $k$  [N/m] is the modal stiffness, and  $y(t)$  [m] is the total tool displacement which consists of the tool modulation  $y_m$  [m] and

displacement by the dynamic cutting force  $y_d$  [m], i.e.,  $y = y_m + y_d$ .  $h(t)$  in Eq. (17) is the uncut chip thickness and should be correctly calculated by considering the generated surface finish. It is calculated based on the surface generated by the maximum tool displacement in previous revolutions as:

$$h(t) = (Y(t) - y_d(t)) - \max\{(Y(t - \tau) - y_d(t - \tau)), (Y(t - 2\tau) - y_d(t - 2\tau))\} \quad (18)$$

Stability of the system can be evaluated by only considering the growth of the dynamic chip thickness  $y_d$ . Specifically, the growing  $y_d$  at the in-cut section is considered as unstable in the simulation. In order to distinguish only this component in the developed time-domain simulator, calculation of tool modulation displacement  $y_m$  is separately carried out, and then it is utilized to calculate  $y_d$ , i.e.,  $y_d = y - y_m$ . This is conducted by solving the following equation of motion:

$$my_m''(t) + cy_m'(t) + ky_m(t) = K_y b(Y(t) - \max\{Y(t - \tau), Y(t - 2\tau)\}) \quad (19)$$

By solving Eqs. (17) and (19),  $y(t)$  and  $y_m(t)$  can be obtained. The solutions are approximated by a 4th order Runge-Kutta method, and displacement is kept in the memory at each calculation step of the time-domain simulation. In order to calculate  $h(t)$  correctly, finding the moment of  $K$ -revolutions before at the same spindle angular position is critical. For instance, when assuming the present data point in the simulation at time  $t$  as  $N_t$ , the data point of  $K$ -revolutions before at the same spindle phase  $N_{t-K\tau}$  is calculated as:

$$N_{t-K\tau} = N_t - \frac{K\tau}{t_{res}} = N_t - \frac{60K}{nt_{res}} \quad (20)$$

where  $t_{res}$  [s] is the time resolution of the simulation. In the simulation, the tool disengagement from the workpiece, i.e.,  $h(t) < 0$ , occurs not only due to the tool modulation but also due to the chatter growth. The cutting force in those situations are defined as zero. Note that chatter vibrations are initiated due to the initial vibration that occurs when the tool engages the workpiece at the beginning of the simulation.

Parameters utilized in the frequency-domain based stability prediction and the time-domain simulation are given in Table 1. In the time-domain simulation, the discretization step  $t_{res}$  [s] is set small enough, e.g. 10  $\mu$ s to realize good accuracy. The cutting width is searched in 0.1 mm increments to detect when chatter starts to grow, and consequently the stability limit  $b_{lim}$  [mm] is determined by subtracting one increment from that width.

Fig. 6 shows an example of the results of the time-domain simulation in stable and unstable conditions. The cutting width in the stable and unstable conditions are 0.5 mm and 4.0 mm, respectively. The cutting conditions and tool modulation parameters of the two conditions are the

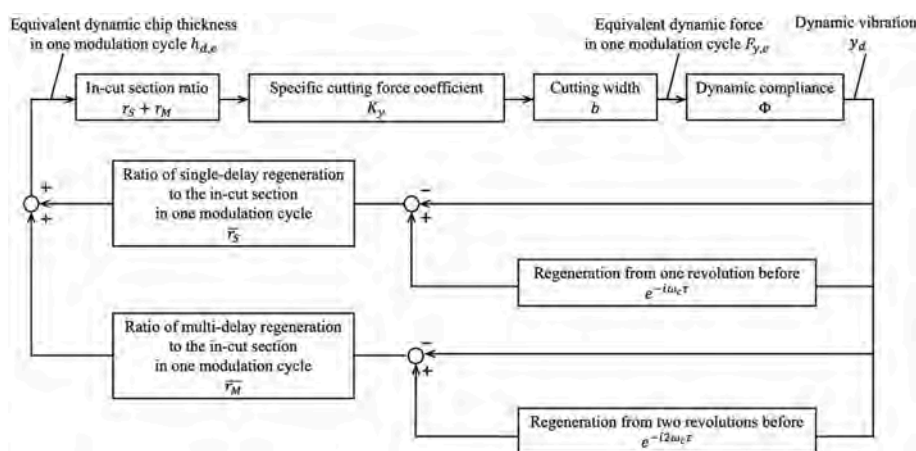


Fig. 5. Block diagram of regenerative chatter in modulated turning process under  $\varphi = \pi$  considering angular length ratio of two regenerative effects and in-cut section ratio.

**Table 1**

Parameters used in proposed chatter stability prediction analysis and time-domain simulation.

Workpiece properties		
Diameter $D$	[mm]	70
Specific cutting force in feed direction $K_y$	[MPa]	711
Modal parameters		
Mass $m$	[kg]	0.2266
Damping coefficient $c$	[N/(m·s)]	44.19
Stiffness $k$	[N/m]	$1.118 \times 10^7$
Cutting conditions		
Spindle speed $n$	[min $^{-1}$ ]	1400–2100
Static feed rate (static depth of cut) $h_0$	[mm/rev]	0.05
Tool modulation parameters		
Ratio of tool modulation frequency to spindle rotation frequency $f_m/f_w$		1.50–3.50
Ratio of tool modulation amplitude to static feed rate $A/h_0$		0.67–2.00
Time-domain simulation conditions		
Increment of cutting width in time-domain simulation	[mm]	0.01
Calculation step (resolution of time-domain simulation)	[μs]	10

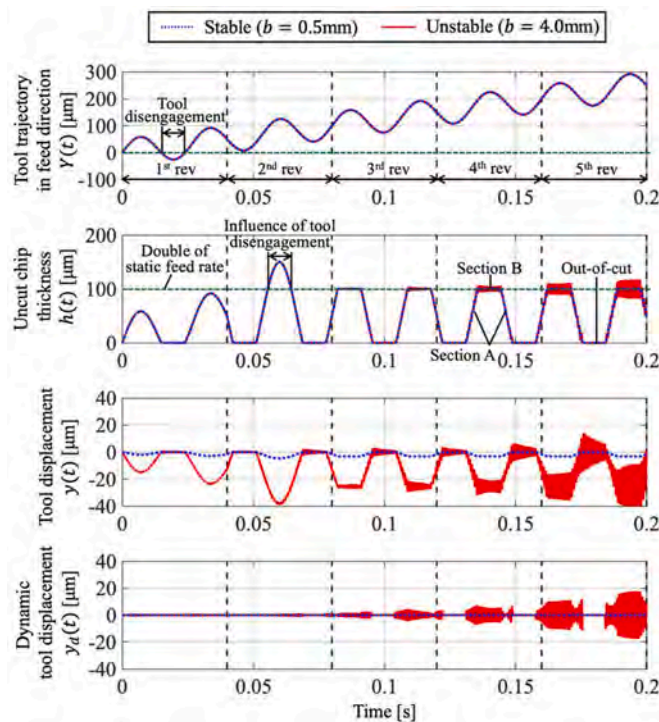


Fig. 6. Example of results of time-domain simulation in stable ( $b = 0.5\text{mm}$ ) and unstable ( $b = 4.0\text{mm}$ ) conditions at  $n = 1500 \text{ min}^{-1}$ ,  $f_m/f_w = 1.5$ , and  $A/h_0 = 1.0$ .

same as  $n = 1500 \text{ min}^{-1}$ ,  $f_m/f_w = 1.5$ , and  $A/h_0 = 1.0$ . As shown in  $Y(t)$ , the tool disengagement occurs in the 1st revolution since the tool modulation amplitude exceeds the static feed, and hence no traces are left on the workpiece in that section. Therefore,  $h(t)$  at that section in the 2nd revolution shows a greater value than double of the static feed rate. From the 3rd revolution, cyclical profiles are obtained with every two revolutions when the system is stable. On the other hand,  $y_d(t)$  keeps growing in every in-cut section when the system is unstable. Observing  $y_d(t)$  allows us to evaluate system stability accurately efficiently, which

is a contribution of the developed time-domain simulator.

### 3. Study on the effect of modulation parameters on process stability

This section investigates on the effects of modulation parameters on regenerative chatter stability of the process. In particular, the influence of single and multiple-delay regenerations on the chatter stability is analyzed.

#### 3.1. Effect of modulation parameters

Firstly, the developed analytical chatter stability model is validated against time domain simulations and effects of modulations parameters such as  $f_m/f_w$  and  $A/h_0$  are investigated. Simulation conditions are given in Table 1, and resultant stability lobe diagrams are provided in Fig. 7. As observed, when tool modulation is applied, chatter stability limit increases for all the modulation frequencies and amplitudes. Red circles indicate time-domain validated stability limits when modulation is applied. Note that time-domain validations are only undertaken for  $n = 1500 \text{ min}^{-1}$ ,  $1750 \text{ min}^{-1}$ , and  $2000 \text{ min}^{-1}$ . Table 2 summarizes stability limits predicted by the frequency-domain analysis, denoted by  $b_{lim,f}$ , and the ones found by the time-domain simulation, denoted by  $b_{lim,t}$ . As shown, proposed frequency domain model predicts process stability fairly accurately.

The stability of modulated turning is influenced by the modulation conditions greatly. Especially, the single and multiple-delay regeneration effects and the out-of-cut duration within a cutting cycle play a critical role in process stability. Fig. 8 shows angular length ratios  $r_s$ ,  $r_M$ ,  $r_O$ , and  $r_s + r_M$  against the  $f_m/f_w$  and  $A/h_0$ .

- 1) For a fixed  $f_m/f_w$ , the predicted/found stability limit by frequency and time domain models,  $b_{lim,f}$  and  $b_{lim,t}$  increase with increasing modulation amplitude ratio,  $A/h_0$ . Thus, it leads to higher stability by utilizing a large tool modulation amplitude. The reason for this can be explained as follows. As shown in Fig. 8, the in-cut section ratio,  $r_s + r_M$ , decreases with the increase of  $A/h_0$  for the same  $f_m/f_w$ . As a result, overall dynamic cutting force decreases since the time for the tool to be in-cut within a tool modulation cycle becomes less. Hence, larger stability limit can be obtained as indicated by Eq. (16). In particular, stability limit when  $A/h_0$  is 0.67, 1.00, and 2.00 increases by about 48.89%, 69.84%, and 85.23% compared to the stability limits without tool modulation. From these results, it can be confirmed that tool modulation is an effective technique to improve the chatter stability. Especially, stability limit can be increased with larger modulation amplitudes at the expense of an increased surface roughness.
- 2) Next, for a fixed  $A/h_0$ , there are no significant changes in the stability for varying  $f_m/f_w$ . It can be observed that the tool modulation frequency does not affect the chatter stability significantly. The reason for this can be explained as follows. Notice from Fig. 8 that  $r_s$ ,  $r_M$ , and  $r_O$  are constant even if  $f_m/f_w$  changes but  $A/h_0$  is constant, i.e., the in-cut duration ratio as well as the out-of-cut duration ratio do not change. In order to confirm these relations quantitatively, the comparison of the summed section length where the out-of-cut occurs per one cycle, i.e., sum of shaded sections in Fig. 9, under different  $f_m/f_w$  are carried out. It is confirmed that  $3\theta_{m,b} = 5\theta_{m,b'}$  between Fig. 9 (b) and 9(b'), and  $3\theta_{m,c} = 5\theta_{m,c'}$  between Fig. 9 (c) and 9(c'). From these results,  $f_m/f_w$  does not affect  $b_{lim,f}$  because there are no changes in  $(r_s + r_M)$  and  $\{\bar{r}_S(e^{-ie_s} - 1) + \bar{r}_M(e^{-ie_M} - 1)\}$  as also indicated in Eq. (16).
- 3) When  $A/h_0$  is smaller than or equal to 0.50, tool always engages into the workpiece, and thus discrete cutting cannot be realized as also shown in Fig. 9(a) and (a'). It denotes  $r_s = 1$ ,  $r_M = 0$ , and  $r_O = 0$ . Therefore, stability limit with tool modulation under those condition

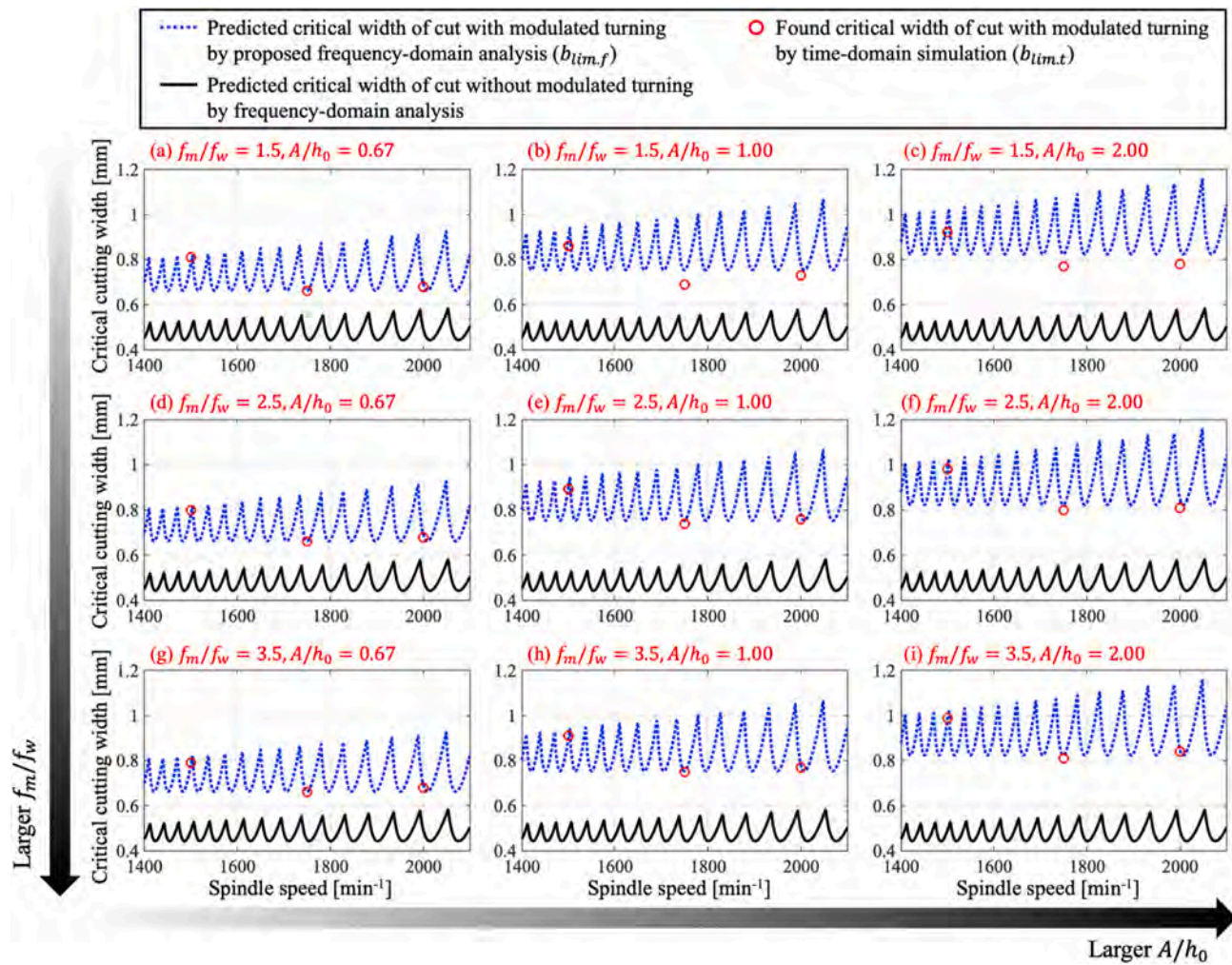


Fig. 7. Predicted/found critical width of cut by proposed frequency-domain analysis and time-domain simulation.

Table 2

Stability limits by proposed frequency-domain analysis and time-domain simulation.

$f_m/f_w, A/h_0$	(a) 1.5, 0.67			(b) 1.5, 1.00			(c) 1.5, 2.00		
$n$ [min <sup>-1</sup> ]	1500	1750	2000	1500	1750	2000	1500	1750	2000
$b_{lim,f}$ [mm]	0.78	0.66	0.69	0.90	0.75	0.78	0.98	0.82	0.85
$b_{lim,t}$ [mm]	0.81	0.66	0.68	0.86	0.69	0.73	0.92	0.77	0.78
$f_m/f_w, A/h_0$	(d) 2.5, 0.67			(e) 2.5, 1.00			(f) 2.5, 2.00		
$n$ [min <sup>-1</sup> ]	1500	1750	2000	1500	1750	2000	1500	1750	2000
$b_{lim,f}$ [mm]	0.78	0.66	0.69	0.90	0.75	0.78	0.98	0.82	0.85
$b_{lim,t}$ [mm]	0.80	0.66	0.68	0.89	0.74	0.76	0.98	0.80	0.81
$f_m/f_w, A/h_0$	(g) 3.5, 0.67			(h) 3.5, 1.00			(i) 3.5, 2.00		
$n$ [min <sup>-1</sup> ]	1500	1750	2000	1500	1750	2000	1500	1750	2000
$b_{lim,f}$ [mm]	0.78	0.66	0.69	0.90	0.75	0.78	0.98	0.82	0.85
$b_{lim,t}$ [mm]	0.79	0.66	0.68	0.91	0.75	0.77	0.99	0.81	0.84

is equal to the stability limit without tool modulation, i.e. the conventional turning case.

### 3.2. Effect of stabilizing factors

This section investigates on the two stabilizing factors; namely, the

ratio of multi-delay/single-delay regeneration durations  $r_M/r_S$  and the ratio of in-cut/out-of-cut durations  $(r_S + r_M)/r_O$ . Both factors affect the characteristic equation and alter process dynamics. The former one ( $r_M/r_S$ ) determines the value of  $\{\bar{r}_S(e^{-i\omega_S} - 1) + \bar{r}_M(e^{-i\omega_M} - 1)\}$  and the latter one  $((r_S + r_M)/r_O)$  determines the value of  $(r_S + r_M)$  in the characteristic equation of the system (See Eq. (16)). In order to gain insight on

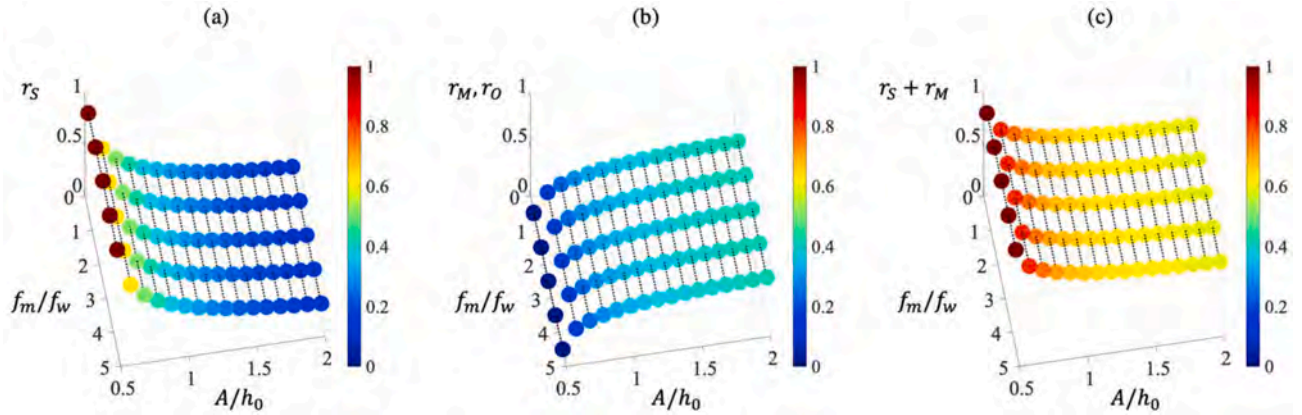


Fig. 8. Angular length ratio in each section per one cycle against modulation parameters  $f_m/f_w$  and  $A/h_0$ : (a)  $r_S$  (b)  $r_M, r_O$  (c)  $r_S + r_M$ .

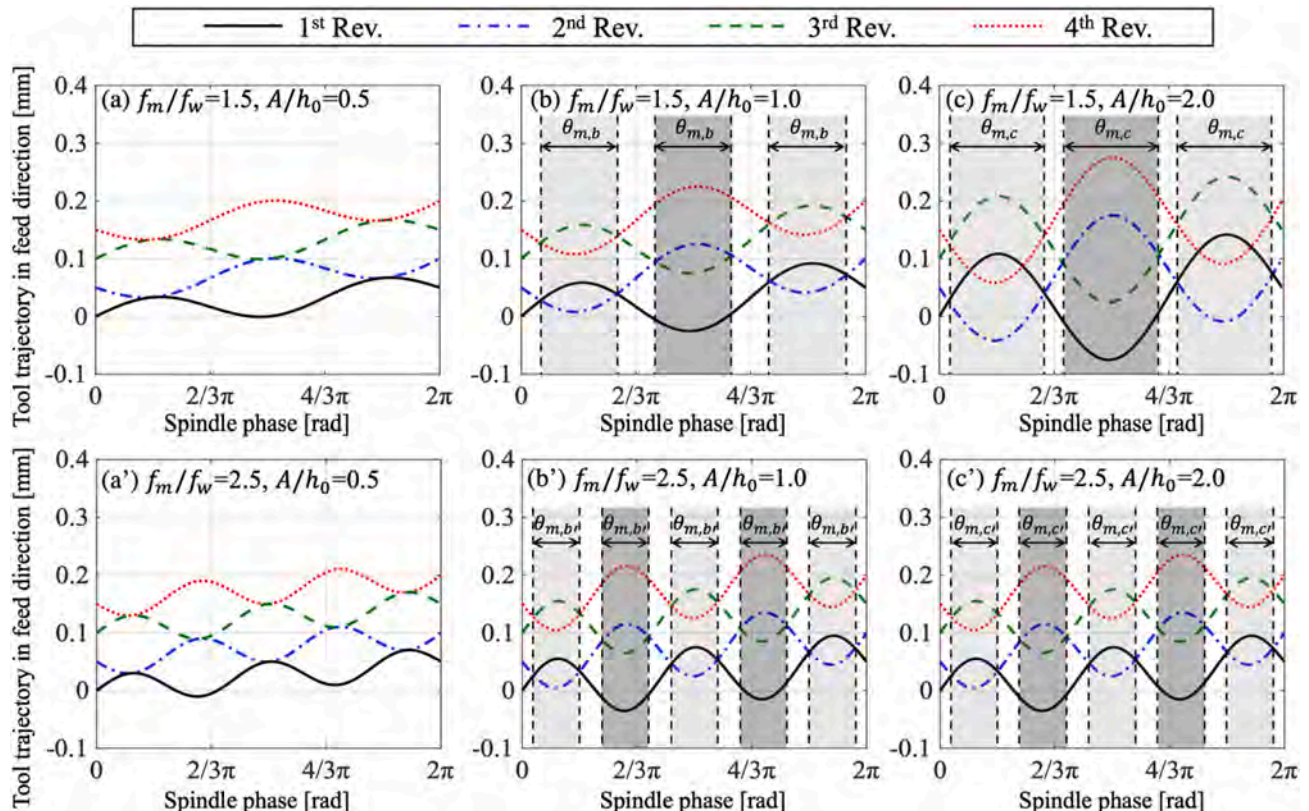


Fig. 9. Tool trajectory in feed direction against spindle phase under various conditions of  $f_m/f_w$  and  $A/h_0$ .

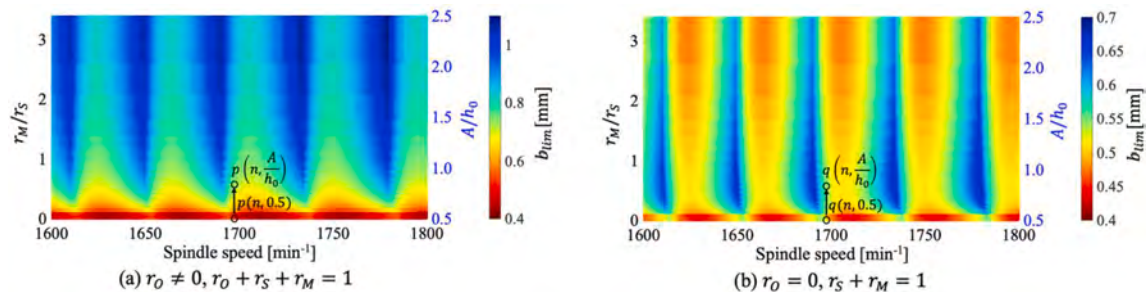


Fig. 10. Results of stability limit analysis: (a) consider effect of out-of-cut duration ( $r_O \neq 0, r_O + r_S + r_M = 1$ ) (b) ignore effect of out-of-cut duration ( $r_O = 0, r_S + r_M = 1$ ).

their effects separately, following analysis is performed.

Firstly, stabilizing effect due to the multi-delay/single-delay regeneration durations is investigated. This is realized by ignoring the effect of out-of-cut duration by forcing  $r_o = 0$  and setting  $r_s + r_M = 1$ . By doing so,  $b_{lim}$  becomes:

$$b_{lim} = \frac{1}{\{\overline{r_s}(e^{-i\omega_s} - 1) + \overline{r_M}(e^{-i\omega_M} - 1)\}K_y\Phi(i\omega_c)} \quad (21)$$

Fig. 10 depicts results of the stability limit analysis based on Eq. (21) for two cases (a) considers the effect of out-of-cut duration by setting  $(r_o \neq 0, r_s + r_M + r_o = 1)$ , whereas (b) ignores the effect of out-of-cut duration ( $r_o = 0, r_s + r_M = 1$ ). Notice that  $r_M/r_s$  becomes larger as  $A/h_0$  becomes larger, and this relationship is shown by the two horizontal axes in Fig. 10. Chatter stability limits with tool modulation without the out-of-cut duration, when  $r_M/r_N = 0$  and  $A/h_0 \leq 0.5$ , are equal to the

stability limits of the conventional continuous cutting. It can be noted from Fig. 10(a) that a higher stability under larger  $A/h_0$  is confirmed, which is the same trend presented in Fig. 7. Meanwhile, from Fig. 10(b), the highest stability limit in each spindle speed is confirmed at specific optimal values of  $r_M/r_s$  or  $A/h_0$ . Specifically, the range of the optimal values of  $r_M/r_s$  and  $A/h_0$  in all spindle speeds are confirmed as  $0.5129 \leq r_M/r_s \leq 0.7205$  and  $0.7143 \leq A/h_0 \leq 0.8333$ , respectively. Hence, it can be concluded that an optimal ratio of multi-delay/single-delay regeneration durations for each spindle speed exists.

Secondly, magnitudes of the two stabilizing factors are investigated by utilizing the results from Fig. 10. The stability limit at each spindle speed and  $A/h_0$  in Fig. 10(a) is defined as  $p(n, A/h_0)$  and similarly for Fig. 10(b) it is defined as  $q(n, A/h_0)$ . The ratio of the stability limits with tool modulation and without tool modulation are calculated as  $p(n, A/h_0)/p(n, 0.5)$ . Note that such ratio makes sense since  $p(n, 0.5)$  is the

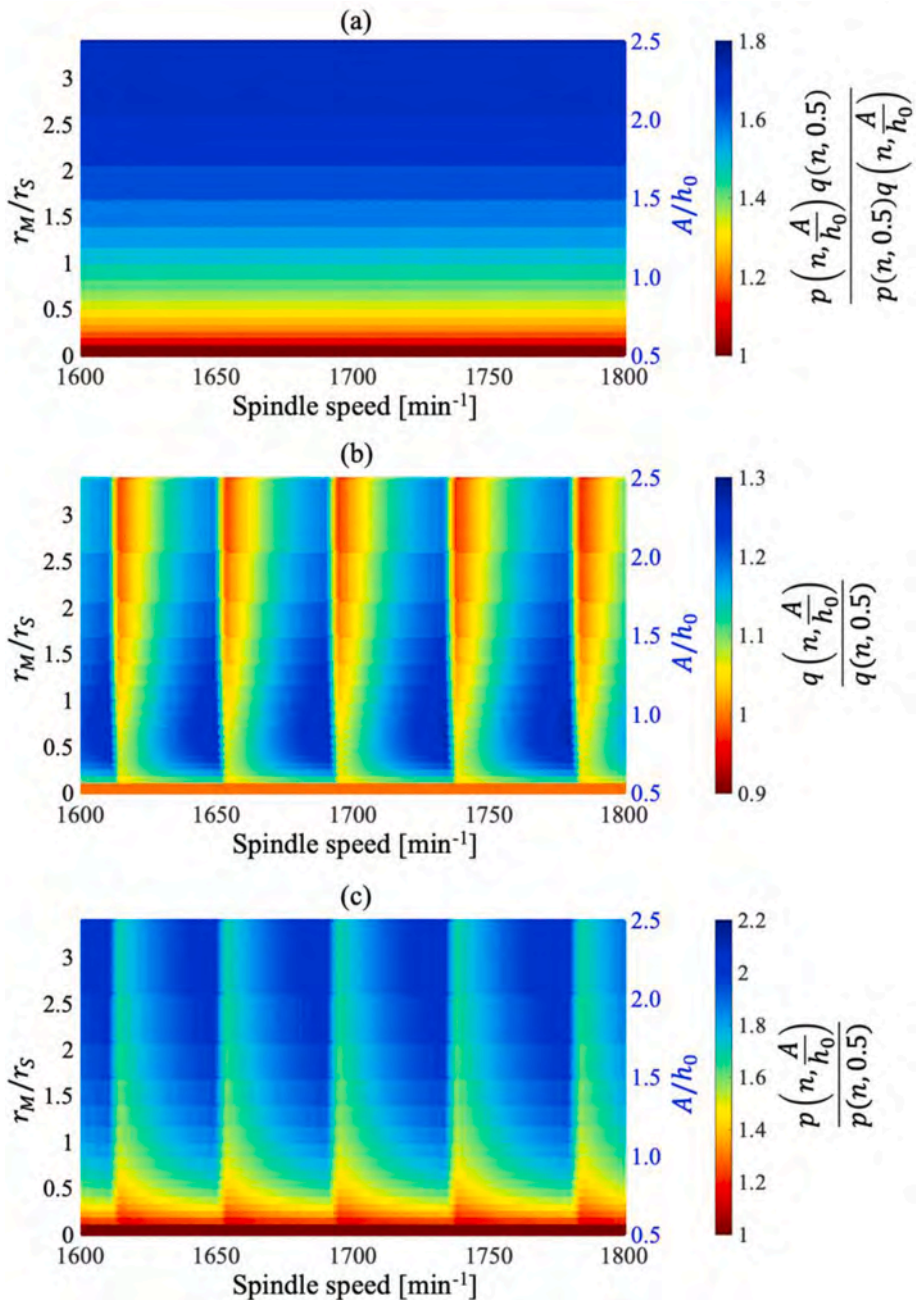


Fig. 11. Increased stability limit ratio by tool modulation: (a) By ratio of in-cut/out-of-cut durations (b) By ratio of multi-delay/single-delay regeneration durations (c) By two stabilizing factors.

stability limit without modulation. In the same manner, the stability increase by the ratio of multi-delay/single-delay regeneration durations  $r_M/r_S$  can be expressed as the ratio  $q(n, A/h_0)/q(n, 0.5)$ , and the stability increase by the ratio of the in-cut/out-of-cut durations  $(r_S + r_M)/r_O$  are expressed as the ratio  $\{p(n, A/h_0)q(n, 0.5)\}/\{p(n, 0.5)q(n, A/h_0)\}$ . Fig. 11 summarizes the increased stability limit ratio by tool modulation compared to without tool modulation. Fig. 11(a) illustrates the increased ratio from in-cut/out-of-cut durations  $\{p(n, A/h_0)q(n, 0.5)\}/\{p(n, 0.5)q(n, A/h_0)\}$  whereas Fig. 11(b) shows the increased ratio from multi-delay/single-delay regeneration durations  $q(n, A/h_0)/q(n, 0.5)$ , and finally Fig. 11(c) is generated by multiplying the results of Fig. 11(a) and (b) as:

$$\frac{p\left(n, \frac{A}{h_0}\right)}{p(n, 0.5)} = \frac{q\left(n, \frac{A}{h_0}\right)}{q(n, 0.5)} \times \frac{p\left(n, \frac{A}{h_0}\right)q(n, 0.5)}{p(n, 0.5)q\left(n, \frac{A}{h_0}\right)} \quad (22)$$

As shown in Fig. 11(a), stability limit is increased by a larger  $A/h_0$  or  $r_M/r_N$ , and the increase does not depend on the spindle speed. Since larger  $A/h_0$  leads to a greater  $r_O$ , i.e., decrease in the in-cut duration  $r_S + r_M$ , a higher stability can be achieved. Specifically, increase in the stability limit is proportional to  $1/(r_N + r_M)$ , which is indicated by Eq. (16). When comparing the results shown in Fig. 11(a) and (b), stability limit increases by almost the same ratio under a smaller  $A/h_0$  or  $r_M/r_N$ , e.g., under  $r_M/r_N \cong 0.5$  or  $A/h_0 \cong 0.7$ , due to the two stabilizing factors. However, the ratio of in-cut/out-of-cut durations show a larger effect on the stability with an increase of  $A/h_0$  or  $r_M/r_N$ . As shown in Fig. 11(b), dependency of stability against spindle speed is determined by the ratio of multi-delay/single-delay regeneration durations. From these results, it can be said that the ratio of in-cut/out-of-cut durations has a larger contribution for stabilizing the system. However, it is also important to set an appropriate combination of the spindle speed and modulation parameters so that a phase relation between the multi-delay/single-delay regenerations to stabilize the cutting can be obtained.

#### 4. Experimental validation

##### 4.1. Experimental setup

A series of experiments are carried out to verify the stabilizing effect by modulated turning and the validity of the proposed chatter stability prediction analysis. The experimental setup for orthogonal (tube) cut-

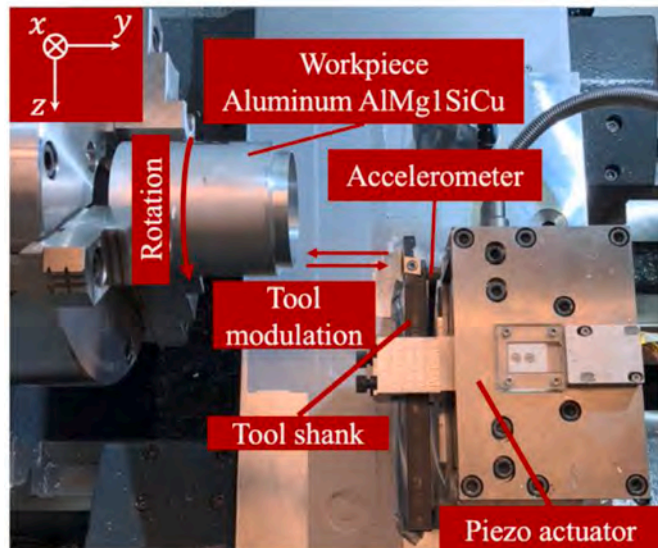


Fig. 12. Experimental setup for pipe-end plunging.

ting is shown in Fig. 12. The experiments are conducted on a CNC lathe (HAAS Automation Inc., TL-1), and an in-house controlled custom-made piezo actuator [36] mounted on the tool-post is utilized to realize the tool modulation in the feed (y) direction. The round pipe (aluminum, ISO AlMg1SiCu) is cut by a tool insert (Kyocera Corp., CCGW09T302 KW10) mounted on a tool shank (Kennametal Inc., steel, SCACR083D) with a square cross-section. The rake and relief angles are 0 and 7 deg, respectively. A PID controller is utilized to control the piezo actuator. The servo position control bandwidth of the piezo actuator is set to 300 Hz for accurate tool modulation. Details on the mechanical design of the piezo actuator are described in Ref. [36]. The actuator is equipped with a capacitive sensor with 5 nm resolution and 25  $\mu\text{m}_{0-p}$  maximum amplitude, and the actuator can provide up to 16000 N. The dynamic stiffness is limited by its 1st resonance mode at 2.97 kHz with 370 N/ $\mu\text{m}$ . An exploded view of the piezo actuator assembly is shown in Fig. 13 [24, 36]. Considering the resonance, the sampling frequency are set highly enough as 10 kHz to catch the force and acceleration signals.

##### 4.2. Measurement of specific cutting force and tool dynamics

Measurement of the specific cutting force and tool dynamic are conducted to utilize its value in the proposed analysis. Since the maximum amplitude of the piezo actuator is limited to 25  $\mu\text{m}_{0-p}$ , the tool modulation amplitude for the cutting experiment is aimed as smaller than or equal to 12  $\mu\text{m}_{0-p}$  in order to secure a sufficient accordance of actual tool modulation with the reference profile. Considering the aimed amplitude range, the static feed rate is set varied from 2.0  $\mu\text{m}/\text{rev}$  to 12.0  $\mu\text{m}/\text{rev}$ . The cutting forces in the feed (y) and cutting (x) directions are measured by 3-axis dynamometer (Kistler Corp., 9257B), and the gradient of cutting force against the cross-sectional area of the uncut chip is identified as the specific cutting force, i.e., the edge force is excluded. The specific cutting force in the feed  $K_y$  and cutting  $K_x$  directions are determined through linear fitting, and their values are 1338 MPa and 1537 MPa, respectively.

The dynamic compliances of the tool shank are measured. An impulse hammer (DYTRAN Instrument Inc., 5800SL 9083) is utilized for the force input, and two accelerometers (DYTRAN Instrument Inc., 3035B1 16021 and 3035B1G 15306) are utilized to measure the vibration acceleration in the feed (y) and cutting (x) directions. To achieve higher reliability of the measurement, the impact for each direction is

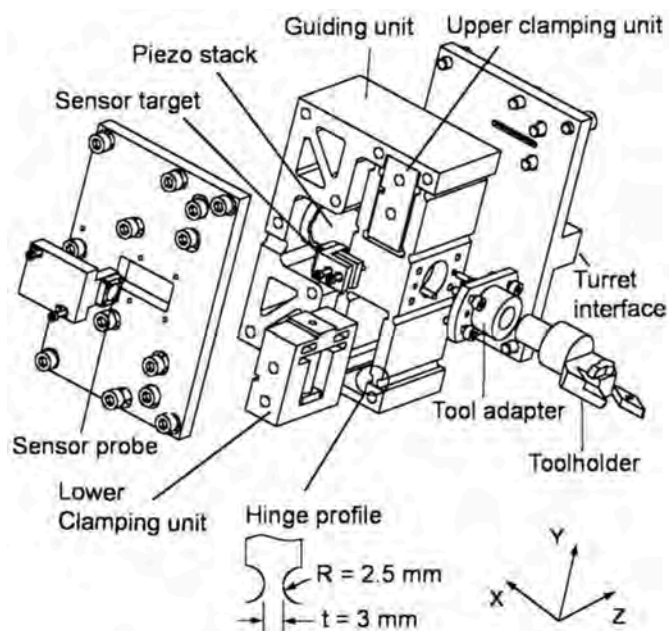


Fig. 13. Exploded view of the piezo actuator assembly [24,36].

repeated 15 times, and their averaged dynamic compliances are calculated. Note that the cutting force in the cutting (x) direction affects the vibration in the feed (y) direction, and hence the equivalent dynamic compliance  $G_y$  [31,32] should be considered for the stability analysis.  $G_y$  is calculated as:

$$G_y = [G_{yx} \ G_{yy}] \begin{bmatrix} K_x/K_y \\ 1 \end{bmatrix} = \frac{K_x}{K_y} \times G_{yx} + G_{yy} \quad (23)$$

where  $G_{yx}$  is the cross dynamic compliance and  $G_{yy}$  is the direct dynamic compliance. The modal parameters of the equivalent dynamic compliance are numerically identified through least-squares fitting against the measured dynamic compliances. As a result, the modal mass  $M_y$  [kg], the modal damping coefficient  $C_y$  [N/(m·s)], and the modal stiffness  $K_y$  [N/m] of  $G_y$  are identified as:  $M_y = 0.0328$ ,  $C_y = 47.15$ , and  $K_y = 8.161 \times 10^6$ . The measured and fitted dynamic compliances are represented by the blue dotted lines and the red solid lines in Fig. 14, respectively. It can be observed that the actual tool compliance can be captured with a good accuracy.

#### 4.3. Cutting experiments and chatter tests

Cutting experiments are carried out to confirm the stabilizing effect of modulated turning as well as to verify the validity of the proposed analysis. The experimental conditions for cutting are shown in Table 3. The cutting width is changed by pre-cut of the pipe thickness of the workpiece. The actual tool modulation profile is directly obtained from a capacitive sensor fastened to the fixed top plate as shown in Fig. 13 [36]. Before the cutting experiments, every actual tool modulation profile is validated against the reference profile to be certain with their accordance. For the calculation of the stability limits by the proposed analysis, the identified modal parameters of the equivalent dynamic compliance are utilized.

Fig. 15 shows the predicted stability limit by the proposed analysis and the experimental results. Short-time Fourier analysis of the measured accelerometer signals is conducted, and the acceleration amplitude obtained at each frequency is converted to the displacement amplitude to investigate into the vibratory behavior of the tool.

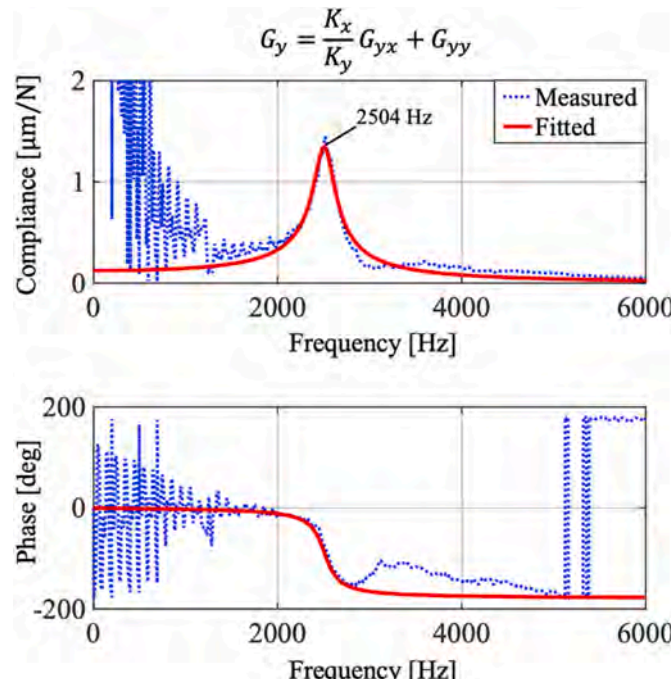


Fig. 14. Measured and fitted equivalent dynamic compliances.

**Table 3**  
Experimental conditions for cutting.

Workpiece properties		
Material		Aluminum ISO AlMg1SiCu
Diameter $D$	[mm]	75
Tool properties		
Projection length	[mm]	47
Cutting conditions		
Spindle speed $n$	[min <sup>-1</sup> ]	1680, 1740, 1800
Cutting speed	[m/min]	396, 410, 424
Cutting width $b$	[mm]	0.5, 0.6, 0.8, 1.0
Static feed rate (static depth of cut) $h_0$	[μm/rev]	4.0
Tool modulation parameters		
Ratio of tool modulation frequency to spindle rotation frequency $f_m/f_w$		1.5, 2.5, 3.5
Ratio of tool modulation amplitude to static feed rate $A/h_0$		0.75, 2.0, 3.0

Experimental chatter stability is judged by the displacement amplitude as follows:  $\circ$  no chatter ( $a_{max} < 5 \mu m_{0-p}$ ),  $\triangle$  slight chatter ( $5 \mu m_{0-p} \leq a_{max} < 10 \mu m_{0-p}$ ), and  $\times$  chatter ( $10 \mu m_{0-p} \leq a_{max}$ ) where  $a_{max}$  is the maximum vibration displacement among the frequency components. The value of the stability limit analysis results with tool modulation at  $n = 1680$ ,  $1740$ , and  $1800 \text{ min}^{-1}$ , which are the spindle speed conditions in the cutting experiments are written in Fig. 15(B-d)-15(B-f). Note that those values are identical even if  $f_m/f_w$  changes. The following remarks which have been found from the simulation are confirmed as follows:

- 1) As shown in Fig. 15(A), the stability limit without tool modulation (conventional turning) is predicted as nearly 0.6 mm regardless of the spindle speed. Since the resonance frequency of the tool shank is as high as about 2.5 kHz as shown in Fig. 14, there is almost no change in the stability limits with spindle speed. The cutting results agree well with the predicted stability limits, and this denotes the validity of not only the measured specific cutting forces but also the utilized modal parameters of the equivalent dynamic compliance.
- 2) It can be confirmed that the chatter vibration is successfully suppressed at 0.8 mm under all the conditions by utilizing tool modulation whereas the chatter growth is confirmed in that width of cut when cutting without tool modulation.
- 3) The increase of the stability limit with an increase of  $A/h_0$  is confirmed from the experimental results under  $f_m/f_w = 3.5$ . This validates the stabilizing effect of tool modulation.
- 4) When  $A/h_0$  is fixed, the predicted stability limits do not alter with different  $f_m/f_w$ . From the cutting experiment results, when  $A/h_0$  is fixed as 3.0, it is confirmed that the stability limit is highest when  $f_m/f_w = 3.5$ . Fig. 16 shows the experimental signals of the cutting force, the vibration acceleration, and the short-time Fourier transform result of the vibration under the cutting conditions marked on Fig. 15: (a) P in Fig. 15 and (b) Q in Fig. 15.
- 5) From the results of the short-time Fourier transform,  $a_{max}$  drastically decreases when  $f_m/f_w$  is increased under  $A/h_0 = 3.0$ . This result can be explained as follows. When the tool stays longer in the continuous in-cut section under smaller  $f_m/f_w$  conditions, it makes the process more prone to growth of chatter.

From the fact that the analytical and experimental stability limits agree fairly well and the tendencies in the experimental verification exactly match with those in the analytical investigation, it can be concluded that the proposed chatter stability prediction analysis is valid, and the chatter suppression effect of tool modulation is verified.

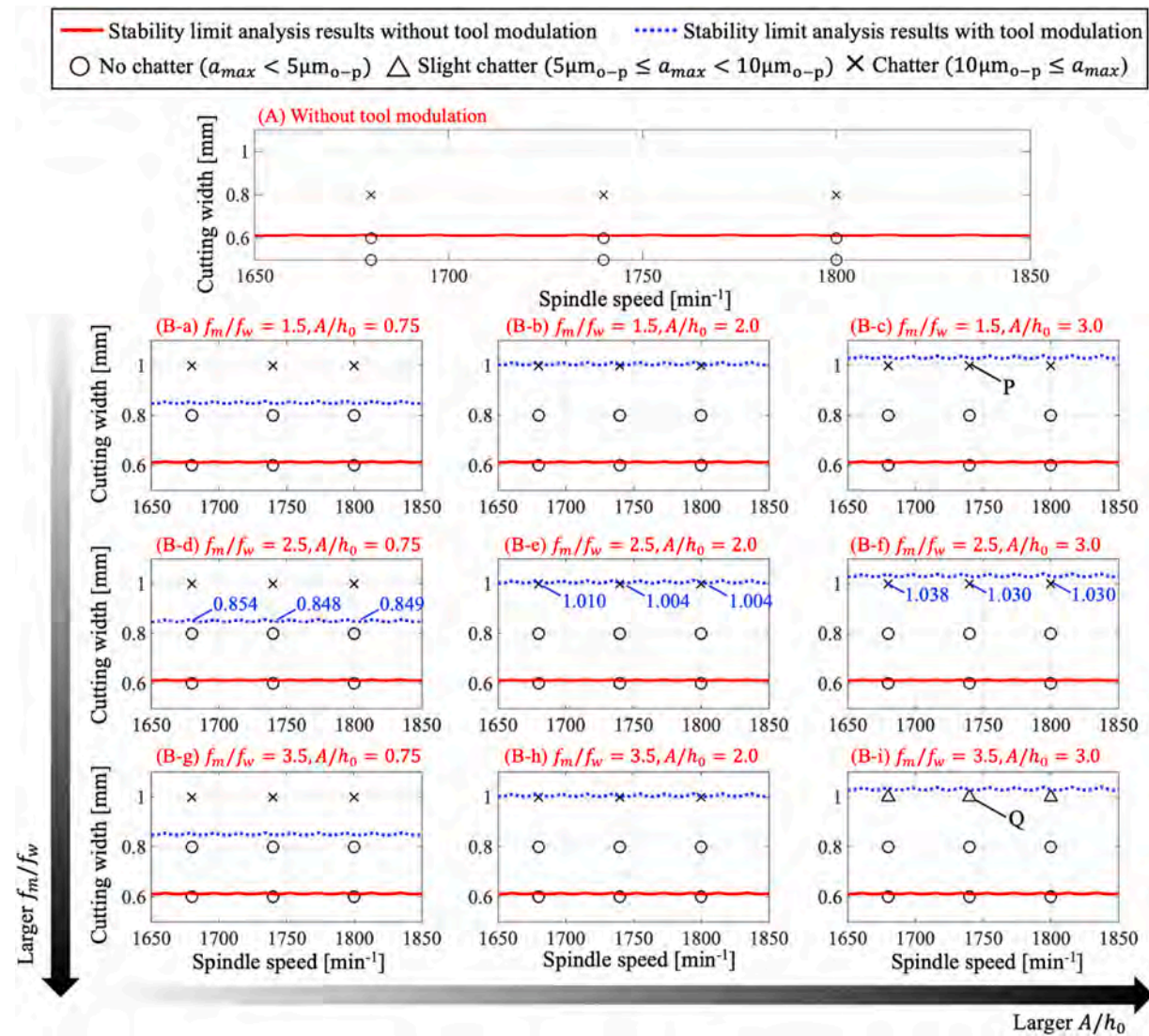


Fig. 15. Stability limit analysis results and experimental results without/with tool modulation under various conditions.

## 5. Conclusion

This paper presented an analytical chatter stability prediction method for modulated turning process. Due to the kinematics of modulated turning, intermittent tool engagement is achieved when tool modulation amplitude exceeds a certain value. As opposed to the milling process, intermittent tool engagement in modulated turning exhibits two phases which are the in-cut (tool engagement) phase and the out-of-cut (tool disengagement) phase. There is no vibration growth in the system during the out-of-cut phase, and only the in-cut phase contributes to the chatter growth. Therefore, the ratio of in-cut and out-of-cut durations affect the chatter stability. When the tool cuts the angular position where the tool disengagement occurred in the previous revolution, vibration that has occurred two spindle revolutions before regenerates. The phase delay of the chatter vibration between these consecutive revolutions can become plural, i.e., multi-delay regeneration can be observed as a novel regeneration mechanism in the modulated turning process. The developed analytical chatter stability prediction method takes above regeneration and delay effects into account to accurately predict the stability of the process. In addition, a time-domain simulator was developed to verify the effectiveness of the proposed analytical chatter prediction approach.

Simulations were conducted to investigate into chatter stability of

the process in detail. Firstly, effects of the tool modulation parameters on the chatter stability were investigated analytically. Effect of two key modulation parameters were considered. The first one is the ratio of the tool modulation frequency to the spindle rotation frequency  $f_m/f_w$ , and the second one is the ratio of the tool modulation amplitude to the static feed rate  $A/h_0$ . The following conclusions are drawn based on the analytical investigations.

- 1) For a fixed  $f_m/f_w$  ratio is constant, chatter stability increases with increasing  $A/h_0$ . Higher stability can be obtained when utilizing a larger tool modulation amplitude. Larger tool modulation amplitude mainly decreases the in-cut section ratio in one modulation cycle. In particular, stability limit with tool modulation under the condition of  $A/h_0 = 2.00$  provides  $\sim 85.23\%$  higher stability margins as compared to the continuous conventional turning. Hence, it was confirmed that modulated turning is an effective technique to improve chatter stability for turning processes.
- 2) For a fixed  $A/h_0$ , there is no significant change in the stability limit under varying modulation frequency,  $f_m/f_w$  conditions. Thus, tool modulation frequency does not greatly affect chatter stability. It was confirmed that the in-cut duration ratio does not change with the  $f_m/f_w$  and so it does not influence the stability.

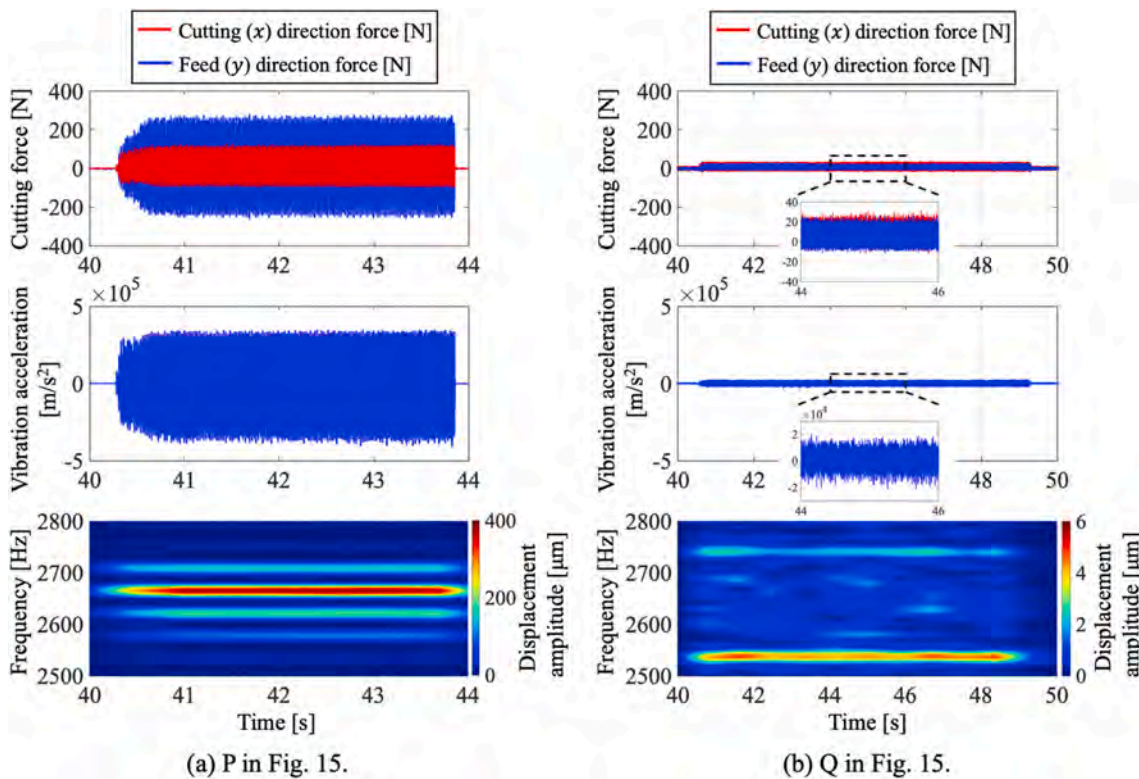


**Fig. 16.** Experimental signals of cutting force, vibration acceleration, and short-time Fourier transform result of vibration under experimental conditions marked on Fig. 15: (a) P and (b) Q.

3) Finally, when  $A/h_0$  is smaller than or equal to 0.50, tool does not disengage from the workpiece, and thus discrete cutting cannot be realized. For this case, stability limits of modulated turning are identical to the conventional continuous turning.

Secondly, the magnitude of the stabilizing effects by the ratio of in-cut/out-of-cut durations and the ratio of multi-delay/single-delay regeneration durations were investigated in frequency domain analysis. It was understood that the effect of in-cut/out-of-cut duration ratio is more significant than the ratio of multi-delay/single-delay regeneration durations. The smaller the ratio of in-cut/out-of-cut durations, the larger the stability limit regardless of spindle speed. This is because the dynamic cutting force decays when the tool is out of cut. On the other hand, an optimal ratio of multi-delay/single-delay regeneration durations exist in each spindle speed. In order to achieve the highest stability limit, it is important to set appropriate combinations of the spindle speed and the tool modulation amplitude.

A series of experiments were carried out to understand the stabilizing effects in modulated turning, and validity of the proposed chatter stability prediction analysis was verified. The proposed analysis greatly contributes to the understanding of chatter suppression mechanism in modulated turning.

#### Credit author statement

Name: Soohyun NamRole: Conceptualization, Methodology, Software, Validation, Formal analysis, Investigation, Writing – Original Draft, Writing – Review & Editing, Visualization, Supervision -2nd author Name: Bora ErenRole: Validation, Investigation, Writing – Review & Editing, Visualization -3rd author Name: Takehiro HayasakaRole: Writing – Review & Editing, Supervision -4th author Name: Burak SencerRole: Writing – Conceptualization, Review & Editing, Supervision, Project administration -5th author Name: Eiji ShamotoRole: Writing – Conceptualization, Review & Editing, Supervision, Project

administration.

#### Declaration of competing interest

The authors declare that they have no known competing financial interests or personal relationships that could have appeared to influence the work reported in this paper.

#### Acknowledgement

This research is supported by the Nagoya University's Graduate Program for Real-world Data Circulation Leaders and US's National Science Foundation (Award no: 2019370).

#### References

- [1] I.S. Jawahir, C.A. Van Luttervelt, Recent developments in chip control research and applications, *CIRP annals* 42 (2) (1993) 659–693.
- [2] I.S. Jawahir, The chip control factor in machinability assessments: recent trends, *J. Mech. Work. Technol.* 17 (1988) 213–224.
- [3] I.S. Jawahir, X.D. Fang, A knowledge-based approach for designing effective grooved chip breakers—2D and 3D chip flow, chip curl and chip breaking, *Int. J. Adv. Manuf. Technol.* 10 (4) (1995) 225–239.
- [4] A.R. Machado, J. Wallbank, I.R. Pashby, E.O. Ezugwu, Tool performance and chip control when machining Ti6Al4V and Inconel 901 using high pressure coolant supply, *Mach. Sci. Technol.* 2 (1) (1998) 1–12.
- [5] A.R. Machado, J. Wallbank, I.R. Pashby, E.O. Ezugwu, Tool performance and chip control when machining Ti6Al4V and Inconel 901 using high pressure coolant supply, *Mach. Sci. Technol.* 2 (1) (1998) 1–12.
- [6] E. Shamoto, T. Aoki, B. Sencer, N. Suzuki, R. Hino, T. Koide, Control of chip flow with guide grooves for continuous chip disposal and chip-pulling turning, *CIRP annals* 60 (1) (2011) 125–128.
- [7] Tomoya Aoki, Burak Sencer, Eiji Shamoto, Norikazu Suzuki, Tomio Koide, Development of a high-performance chip-guiding turning process—tool design and chip flow control, *Int. J. Adv. Manuf. Technol.* 85 (1) (2016) 791–805.
- [8] P.N. Chhabra, B. Ackroyd, W.D. Compton, S. Chandrasekar, Low-frequency modulation-assisted drilling using linear drives, *Proc. IME B J. Eng. Manufact.* 216 (3) (2002) 321–330.
- [9] Lídia Simão, Ana Lisboa, Green marketing and green brand—The Toyota Case, *Procedia manufacturing* 12 (2017) 183–194.

[10] Ryan Copenhaver, Tony Schmitz, Modeling and simulation of modulated tool path (MTP) turning stability, *Manufacturing Letters* 24 (2020) 67–71.

[11] Luke Berglind, John Ziegert, Modulated tool path (MTP) machining for threading applications, *Procedia manufacturing* 1 (2015) 546–555.

[12] Yang Guo, James B. Mann, Control of chip formation and improved chip ejection in drilling with modulation-assisted machining, *J. Manuf. Sci. Eng.* 142 (2020) 7.

[13] Juan Sandoval, Dinh Nguyen, Patrick Kwon, Yang Guo, An experimental study of modulation-assisted turning of Ti6Al4V, in: *International Manufacturing Science and Engineering Conference* vol. 58752, American Society of Mechanical Engineers, 2019. V002T03A063.

[14] Yang Guo, Stalbaum Tyler, James Mann, Yeung Ho, Srinivasan Chandrasekar, Modulation-assisted high speed machining of compacted graphite iron (CGI), *J. Manuf. Process.* 15 (4) (2013) 426–431.

[15] J.B. Mann, Y. Guo, C. Saldana, W.D. Compton, S. Chandrasekar, Enhancing material removal processes using modulation-assisted machining, *Tribol. Int.* 44 (10) (2011) 1225–1235.

[16] James B. Mann, Yang Guo, Christopher Saldana, Yeung Ho, W. Dale Compton, Srinivasan Chandrasekar, Modulation-assisted machining: a new paradigm in material removal processes, in: *Advanced Materials Research* vol. 223, Trans Tech Publications Ltd, 2011, pp. 514–522.

[17] Ho Yeung, Yang Guo, Narayan K. Sundaram, James B. Mann, W. Dale Compton, Srinivasan Chandrasekar, Mechanics of modulation assisted machining, in: *ASME 2013 International Manufacturing Science and Engineering Conference Collocated with the 41st North American Manufacturing Research Conference*, American Society of Mechanical Engineers Digital Collection, 2013.

[18] Xavier Beudaert, Asier Astarloa, Jesus Alvarez, Maria Helena Fernandes, Jokin Munoa, *Chip Breaking System for Turning Applications Using Machine Drive Oscillations*, 2017.

[19] Yang Guo, Seong EYL Lee, James B. Mann, Piezo-actuated modulation-assisted drilling system with integrated force sensing, *J. Manuf. Sci. Eng.* 139 (2017) 1.

[20] H.G. Toews Iii, W.D. Compton, S. Chandrasekar, A study of the influence of superimposed low-frequency modulation on the drilling process, *Precis. Eng.* 22 (1) (1998) 1–9.

[21] Yang Guo, James B. Mann, Experimental evaluation of cutting kinematics and chip evacuation in drilling with low-frequency modulation-assisted machining, in: *ASME 2017 12th International Manufacturing Science and Engineering Conference Collocated with the JSME/ASME 2017 6th International Conference on Materials and Processing*, American Society of Mechanical Engineers Digital Collection, 2017.

[22] Ho Yeung, Yang Guo, James B. Mann, W. Dale Compton, Srinivasan Chandrasekar, Effect of low-frequency modulation on deformation and material flow in cutting of metals, *J. Tribol.* 138 (2016) 1.

[23] Y. Gao, R.L. Sun, Y.N. Chen, J. Leopold, Mechanical and thermal modeling of modulation-assisted machining, *Int. J. Adv. Manuf. Technol.* 86 (9) (2016) 2945–2959.

[24] Bora Eren, Burak Sencer, Mechanistic cutting force model and specific cutting energy prediction for modulation assisted machining, *Procedia Manufacturing* 48 (2020) 474–484.

[25] Yuan Gao, Ronglei Sun, Yanni Chen, Jürgen Leopold, Analysis of chip morphology and surface topography in modulation assisted machining, *Int. J. Mech. Sci.* 111 (2016) 88–100.

[26] Ho Yeung, Narayan K. Sundaram, James B. Mann, W. Dale Compton, Srinivasan Chandrasekar, Energy dissipation in modulation assisted machining, *Int. J. Mach. Tool Manufact.* 74 (2013) 41–49.

[27] S. Smith, B. Woody, W. Barkman, D. Tursky, Temperature control and machine dynamics in chip breaking using CNC toolpaths, *CIRP annals* 58 (1) (2009) 97–100.

[28] Yusuf Altintas, Gabor Stepan, Erhan Budak, Tony Schmitz, Zekai Murat Kilic, Chatter stability of machining operations, *J. Manuf. Sci. Eng.* 142 (2020) 11.

[29] J. Munoa, X. Beudaert, Z. Dombovari, Y. Altintas, Erhan Budak, C. Brecher, G. Stepan, Chatter suppression techniques in metal cutting, *CIRP Annals* 65 (2) (2016) 785–808.

[30] Eiji Shamoto, Shunsuke Fujimaki, Burak Sencer, Norikazu Suzuki, Takashi Kato, Rei Hino, A novel tool path/posture optimization concept to avoid chatter vibration in machining—proposed concept and its verification in turning, *CIRP annals* 61 (1) (2012) 331–334.

[31] S. Nam, T. Hayasaka, H. Jung, E. Shamoto, Proposal of novel chatter stability indices of spindle speed variation based on its chatter growth characteristics, *Precis. Eng.* 62 (2020) 121–133.

[32] S. Nam, T. Hayasaka, H. Jung, E. Shamoto, Proposal of Novel Spindle Speed Variation Profile with Constant Acceleration Rate for Improvement of Chatter Stability, *Precision Engineering*, 2020.

[33] Umut Karagüzel, Emre Uysal, Erhan Budak, Mustafa Bakkal, Analytical modeling of turn-milling process geometry, kinematics and mechanics, *Int. J. Mach. Tool Manufact.* 91 (2015) 24–33.

[34] Ryan Copenhaver, Tony Schmitz, Smith Scott, Stability analysis of modulated tool path turning, *CIRP Annals* 67 (1) (2018) 49–52.

[35] Emre Ozlu, Erhan Budak, Comparison of one-dimensional and multi-dimensional models in stability analysis of turning operations, *Int. J. Mach. Tool Manufact.* 47 (2007) 12–13, 1875–1883.

[36] Y. Altintas, A. Woronko, A piezo tool actuator for precision turning of hardened shafts, *CIRP Annals* 51 (1) (2002) 303–306.